Annals of Biomedical Engineering, Vol. 25, pp. 398–416, 1997
Printed in the USA. All rights reserved.

0090-6964/97 $10.50 + .00
Copyright © 1997 Biomedical Engineering Society

Impulse Response Model in Reconstruction of Insulin Secretion by Deconvolution: Role of Input Design in the Identification Experiment

GIOVANNI SPARACINO AND CLAUDIO COBELLI

Dipartimento di Elettronica ed Informatica, Universita' di Padova, Via Gradenigo 6/A, 35131, Padova, Italy

Abstract—Insulin secretion rate (ISR) *in vivo* can be reconstructed by deconvolution of plasma concentration of C-peptide (CP), a peptide co-secreted with insulin but not extracted by the liver and exhibiting linear kinetics. Deconvolution requires the knowledge of the CP impulse response. A two exponential model is usually chosen to describe the CP impulse response but three exponential and one exponential models have also been used. The purpose of this paper is to investigate the role of the CP impulse response model order in reconstructing ISR by deconvolution in three standard physiological/clinical situations: ultradian oscillations, rapid pulses, and biphasic response to a glucose stimulus. By resorting to simulation, we first show that, in each situation, the validity of impulse response models with different orders depends on the input chosen in the impulse response identification experiment. Real data are then used which support the simulation results.

Keywords—Physiological system, System identification, Model, Simulation, C-peptide.

INTRODUCTION

Insulin is the key hormone in the regulation of glucose metabolism in humans and its secretion by the pancreatic β cells is finely controlled. In normal conditions, insulin secretion is an oscillatory process that involves at least two detectable modes; rapid pulses with periods between 8 and 15 min (8,10) are superimposed on ultradian oscillations that are slower and larger in amplitude, whose periods usually vary between 90 and 150 min (17,19,23). If glucose concentration increases, *e.g.*, as an effect of a glucose stimulus, spontaneous oscillations are obscured by the biphasic response of the pancreas, *i.e.*, a sudden and large first phase secretory peak followed by a smooth second phase release (14,20).

Measuring insulin secretion rate (ISR) is thus essential for understanding β-cell function both in healthy and diabetic subjects. ISR, however, can not be directly assessed *in vivo*. In addition, plasma concentration of insulin does not reflect β-cell secretion, because insulin undergoes a large and variable hepatic extraction before reaching plasma (18). However, a peptide, C-peptide (CP), is co-secreted with insulin on an equimolar basis and is not extracted by the liver (15). Hence, the plasma concentration of CP directly reflects ISR. Because CP kinetics are linear in a wide range of concentrations it is possible to pose the measurement of ISR in man as an input estimation problem that can be solved by deconvolution (6,15,16,19,20,23). Deconvolution requires the CP impulse response. A two exponential impulse response model is usually chosen to describe the CP impulse response (6,7,16,19,20,23,25), but three exponential (22) and one exponential models (26–28) have also been used.

The purpose of this study is to investigate the role of the CP impulse response model order when deconvolution is applied to reconstruct ISR ultradian oscillations, rapid pulses, and biphasic response to a glucose stimulus. By resorting to simulation, we will show how the domain of validity of impulse response models with different orders depends on the frequency used to sample CP plasma concentration and how the input in the impulse response identification experiment is designed. Real data will also be used to assess the simulation results.

SIMULATION DATABASE

Three ISR profiles were simulated to describe ultradian oscillations, rapid pulses, and response to a glucose stimulus. The function used to simulate an ISR

Acknowledgment—Dr. K. Polonsky and Dr. J. Sturis (Department of Medicine, University of Chicago, IL, U.S.A.) kindly provided us the real C-peptide data. This paper was partially supported by MURST project "Bioingegneria dei Sistemi Metabolici e Cellulari" and by National Institutes of Health Grant RR02176 "Resource Facility for Kinetic Analysis."

Address correspondence to Claudio Cobelli, Dipartimento di Elettronica ed Informatica, Universita' di Padova, Via Gradenigo 6/A, 35131 Padova, Italy.

(Received 19Jan96, Revised 24May96, Accepted 20Jun96)

ultradian oscillatory pattern (Fig. 1 A) was:

$$\begin{aligned}\mathrm{ISR}(t) = C + \{A[1 + 0.2\sin(\omega_a t)]\} \\ \times \sin\{[1 + 0.1\sin(\omega_p t)]\omega_s t\} \quad t \le t_M\end{aligned} \tag{1}$$

where C = 80 pmol/min; A = 80 pmol/min; $\omega_a = 2\pi/400$ rad/min; $\omega_p = 2\pi/700$ rad/min; $\omega_s = 2\pi/130$ rad/min; t_M = 800 min.

The same function as Eq. 1, but with C = 80 pmol/min, A = 30 pmol/min, $\omega_a = 2\pi/80$ rad/min, $\omega_p = 2\pi/600$ rad/min, $\omega_s = 2\pi/12$ rad/min, t_M = 130 min, was also used to simulate ISR rapid pulses (Fig. 1 B). *In vivo*, rapid pulses are superimposed on ultradian oscillations, but in this paper, for the sake of convenience and simplicity, we will study the two oscillatory modes separately.

The function used to simulate an ISR profile after a glucose stimulus (Fig. 1 C) was:

$$\mathrm{ISR}(t) = \begin{cases} C & t < 0 \\ C + B_1 e^{-b_1 t} + B_2 e^{-b_2 t} + B_3 t^{p_1} e^{-b_3 t} + B_4 t^{p_2} e^{-b_4 t} & \\ & 0 \le t \le 240 \end{cases} \tag{2}$$

where C = 80 pmol/min; $B_1 = B_2$ = 8000 pmol/min; p_1 = 3; p_2 = 1.75; B_3 = 1.4 pmol/(min)$^{p_1-1}$; B_4 = 1.2 pmol/(min)$^{p_2-1}$; $b_1 = 1.8^{-1}$ min^{-1}; $b_2 = 1.1^{-1}$ min^{-1}; $b_3 = p_1/15$ min^{-1}; $b_4 = p_2/50$ min^{-1}.

The impulse response of the CP system was described by a three exponential model previously identified in (22) on real data taken from (20):

$$g^t(t) = \sum_{i=1}^{3} A_i e^{-\alpha_i t} \tag{3}$$

where superscript t denotes "true"). Table 1 in the Appendix shows the values of the impulse response parameters as well as the values of some key kinetic parameters (1) of the simulated CP system: the steady-state gain K (equal to the reciprocal of the plasma clearance rate), the plasma distribution volume (V), and the mean residence time (MRT) in the system.[1] The time course of $g^t(t)$ is shown in Fig. 1 D.

Simulated CP plasma concentration profiles were obtained by convoluting the input functions with the impulse response. For each ISR, the sampling rates of the CP concentration in plasma were those typically used in practice: uniform with a 10 min period in the ultradian oscillation case, uniform with a 2 min period for rapid pulses, nonuniform with a period varying from 1 min (first phase) to 20 min (second phase) for the response to a glucose stimulus. Figure 1 E, F, and G shows the simulated CP concentration profiles together with their (noise-free) samples.

DECONVOLUTION IN THE FREQUENCY DOMAIN

The study of the role of the impulse response model in a deconvolution problem can be performed conveniently in the frequency domain. To do so we consider, in a deterministic setting and in the uniform sampling case, the Z-transform representation of the discrete-time relation between the input and the output of the system (4).

Let $u(t)$ be the input (ISR) of the CP system having $g^t(t)$ as the impulse response. The output $c(t)$ (CP plasma concentration) is:

$$c(t) = \int_0^t g^t(t - \tau)u(\tau)\, d\tau \tag{4}$$

where, for the sake of simplicity, $u(t) = 0$ for $t < 0$. The concentration sampling schedule is denoted by $\Omega_S = \{kT\}$, $k = 1, 2, \cdots \infty$, T being the sampling period. The kth sample can be expressed as:

$$\begin{aligned} c_k = c(kT) &= \int_0^{kT} g^t(kT - \tau)u(\tau)\, d\tau \\ &= \sum_{i=1}^{k} \int_{(i-1)T}^{iT} g^t(kT - \tau)u(\tau)\, d\tau \end{aligned} \tag{5}$$

Let's approximate $u(t)$ as a piecewise constant on Ω_S, *i.e.*, $u(t) = u_i$ for $(i - 1)T < t < iT$ with $i = 1, 2, \cdots \infty$. From Eq. 5 it follows that:

$$c_k = \sum_{i=1}^{k} u_i \int_{(i-1)T}^{iT} g^t(kT - \tau)\, d\tau \tag{6}$$

where u_i can be also interpreted as the average level of $u(t)$ in the ith sampling interval. Because

$$\int_{(i-1)T}^{iT} g^t(kT - \tau)\, d\tau = \int_{(k-i)T}^{(k-i+1)T} g^t(t)\, dt \tag{7}$$

depends on the difference $(k - i)$ only for $g^t(t)$ and T fixed, having defined:

$$g_p^t = \int_{pT}^{(p+1)T} g(t)\, dt \quad p = 1, 2, \cdots \infty \tag{8}$$

[1] K, the steady-state gain, is equal to AUC (area under the curve) of $g^t(t)$; V, the plasma distribution volume, is computed as $1/g^t(0)$; MRT, the mean residence time, is computed as the ratio of AUC of $tg^t(t)$ over AUC of $g^t(t)$.

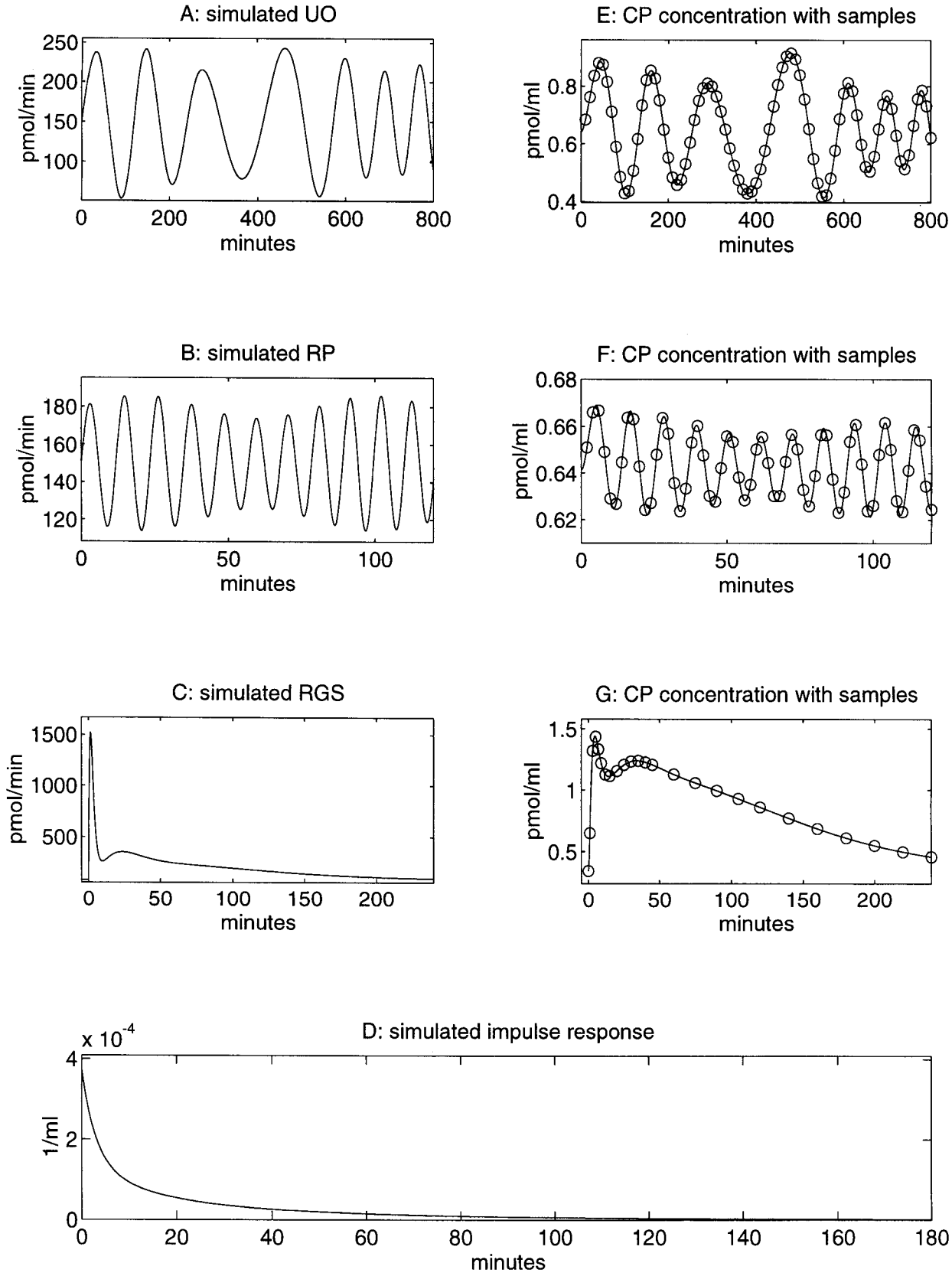

FIGURE 1. The simulation database. (A) Simulated ultradian oscillations (UO). (B) Simulated rapid pulses (RP). (C) Simulated response to a glucose stimulus (RGS). (D) C-peptide (CP) system impulse response. (E) CP concentration and noise-free samples due to insulin secretion rate (ISR) of (A). (F) CP concentration and noise-free samples due to ISR of (B). (G) CP concentration and noise-free samples due to ISR of (C).

one has:

$$c_k = \sum_{i=0}^{k} u_i g^t_{k-i} \quad k = 0, 1, 2, \cdots, \infty \tag{9}$$

where $u_0 = 0$.

Equation 9 is a discrete-time convolution and has the well-known Z-domain counterpart (12):

$$C(z) = G^t(z)U(z) \tag{10}$$

where $U(z)$ and $C(z)$ are the Z-transform of the sequences $\{u_k\}$ and $\{c_k\}$, respectively. $G^t(z)$ is the transfer function of the discrete-time system. In our case $G^t(z)$ is asymptotically stable and minimum phase (12).

The transfer function $G^t(z)$ has an important meaning for $z = e^{j2\pi\nu T}$ (where ν is the frequency, expressed in min^{-1}), *i.e.*, on the unitary circle of the complex plane. In fact, for a stable system, if the input $\{u_k\}$ is a sinusoid with frequency ν_0, with unitary amplitude and zero phase, after a transient the output $\{c_k\}$ will be a sinusoid with frequency ν_0, amplitude $|G^t(e^{j2\pi\nu_0 T})|$, and phase $arg\{G^t(e^{j2\pi\nu_0 T})\}$. The complex function $G^t(e^{j2\pi\nu T})$ is called the frequency response of the system. Note that the frequency response $G^t(e^{j2\pi\nu T})$ is a periodic function in ν with period equal to $1/T$ or, equivalently, $G^t(e^{j\theta})$ is periodic with period equal to 2π, θ being equal to $2\pi\nu T$ (θ expressed in radians). The modulus and the argument of the frequency response are (real) even functions. For the purpose of this paper, it will be sufficient to focus on the modulus of the frequency response $|G^t(e^{j2\pi\nu T})|$ only, which will be referred to as the frequency response. For $\nu = 0$ one has $|G^t(1)|$, the steady-state gain of the system.

$G^t(z)$ depends on both the time continuous impulse response, *i.e.*, $g^t(t)$, and on the sampling period T, see (7). The longer the sampling period T, the more the spectral content of $G^t(e^{j2\pi\nu\tau})$ differs from that of the Fourier transform of $g^t(t)$. In particular, as expected from theory (9,12,13), the longer the sampling period T, the more the high-frequency components of $g^t(t)$ are aliased in the spectrum of the discrete-time system.

In practical applications, the true impulse response $g^t(t)$ is unknown and, in deconvolution, one is forced to use a model, $g^m(t)$, in place of $g^t(t)$. By applying the same rationale that is behind Eq. 10, one can derive $G^m(z)$ from $g^m(t)$, the model of the discrete-time transfer function of the system. In the CP case, because of the small intraindividual variability (25), $g^m(t)$ can be determined by a separate input-output experiment. For instance (16,20), after suppression of pancreatic secretion by somatostatin, an intravenous CP bolus is administered, the decay curve is frequently sampled, and $g^m(t)$ is identified. However, as discussed in the Introduction, three different model orders have been used in the literature to describe the CP impulse response $g^m(t)$.

Assuming no measurement errors affect $\{c_k\}$, $\hat{U}(z)$, *i.e.*, the Z-transform of the sequence of the input estimates $\{\hat{u}_k\}$, can be obtained as:

$$\hat{U}(z) = \frac{C(z)}{G^m(z)} \tag{11}$$

By comparing Eq. 10 with Eq. 11 it follows that deviations of $G^m(z)$ from $G^t(z)$ will obviously produce errors in $\hat{U}(z)$ and thus on $\{\hat{u}_k\}$. In particular, deviations of the model frequency response $G^m(e^{j2\pi\nu T})$ from the true one $G^t(e^{j2\pi\nu T})$ will produce distortions in the spectrum of the deconvoluted input. However, it is important to stress that such distortions will be negligible if $G^m(e^{j2\pi\nu T})$ is close to $G^t(e^{j2\pi\nu T})$ in the band where most of the spectral content of the signals lies, whereas even large differences between $G^m(e^{j2\pi\nu T})$ and $G^t(e^{j2\pi\nu T})$ outside the signals band will play a minor role. In the next section, we will see that the closeness of the model frequency response, *i.e.*, $G^m(e^{j2\pi\nu T})$, to the true system response, *i.e.*, $G^t(e^{j2\pi\nu T})$, does not only depend on sampling rate and model order, but also on the form of the input designed to obtain the impulse response model.

Remark. When the sampling period is not constant, calculations similar to those of Eqs. 4–9 can still be done, but the resulting discrete-time input-output relation is not a convolution sum as in Eq. 9. Our problem would need to be apprached by resorting to the vector-matrix input-output model:

$$c = G^t u \tag{12}$$

where u and c are the n-dimension input and output vector, respectively (assume a fixed number of data n), and G^t is a n-dimension lower triangular square matrix whose (k, i)th element ($k = 1, 2, \cdots n$; $i = 1, \cdots k$) is:

$$G^t(k, i) = \int_{t_{i-1}}^{t_i} g^t(t_k - \tau)\, d\tau \tag{13}$$

where t_k is the kth sampling time ($t_0 = 0$). Similarly to Eq. 11, the input estimate is obtained by solving the linear system (12) with G^m in place of G^t. Investigating this situation would be more difficult than studying the uniform sampling case by using the Z-transform approach, but it would lead to similar conclusions.

ROLE OF IMPULSE RESPONSE MODEL: INFLUENCE OF THE INPUT CHOSEN FOR ITS IDENTIFICATION

Here, we solve the simulated deconvolution problems under "Simulation Database" by using three impulse response model orders, *i.e.*, a one (1E), a two (2E) and a three (3E) exponential model. The parameters of these models will be estimated by nonlinear least squares (1) from the sampled simulated data obtained from $g^t(t)$ by using different inputs. We will consider both standard inputs, *i.e.*, a bolus ("Bolus Input for Impulse Response Identification"), a step infusion ("Step Input for Impulse Response Identification"), a square wave ("Square Wave Input for Impulse Response Identification") and nonstandard ones ("Better Inputs for Impulse Response Identification"). In each experiment, as detailed in the Appendix, the sampling schedule Ω_S used to generate the sampled simulation data is different and appropriate for identifying each model; however, no attempt is made to choose optimal sampling times (2,3). In addition, to solely analyze the role of the impulse response model, we will consider noise-free data. In this way, because ill conditioning cannot come into play in the interpretation of the deconvolution results, we ensure that errors in the estimated ISR will only reflect errors in the impulse response model.

In this section, deconvolution will not be tackled using the Z-transform relation given by Eq. 11, but by a recently proposed nonparametric algorithm (5) particularly suitable to solve our simulated problems. In this paper, Z-transforms do not play an algorithmic but a conceptual role. In fact, Eq. 11 will allow us to assess the role of the model frequency response in deconvolution, independently on the particular deconvolution algorithm in use.

The deconvolution algorithm we adopt, presented in detail in (5), can be described as follows: Because of the ill posedness of the input estimation problem, there are infinite continuous-time functions whose convolution with the impulse response model match the available output data; the algorithm selects the smoothest, *i.e.*, that function having less second time-derivatives energy.

Bolus Input for Impulse Response Identification

Given the true three exponential impulse response $g^t(t)$ (Eq. 3), we generated a decay curve by simulating an experiment in which a bolus input of CP is administered in plasma. We then fitted 1E, 2E, and 3E models against noise-free samples of the decay curve. We considered a different sampling schedule Ω_s for each model. In the Appendix we report the bolus dose, the sampling schedule used for each model, and the value of the estimated impulse response parameters together with the values of the other system kinetic parameters [calculated as in Footnote 1 by using $g^m(t)$ in place of $g^t(t)$].

Three Exponential Model. As expected, the 3E model $g^m(t)$ perfectly performs in reconstructing all the ISR patterns (results not shown).

Two Exponential Model. Figure 2 (top-left panel) shows the 2E model fit against the samples of the simulated decay curve. Figure 2 (top-right panel) displays the difference between the time course of $g^m(t)$ and that of $g^t(t)$. (For sake of clarity we do not show $g^m(t)$ *versus* $g^t(t)$, which would have appeared too close in the first minutes.) Note that $g^m(t)$ does not describe perfectly the first portion of $g^t(t)$, *i.e.*, $g^m(t)$ slightly underestimates the high-frequency components in $g^t(t)$. Figure 2 (middle panel) compares the deconvoluted rapid pulses profile with the true one and highlights the deficiency of the 2E model at high frequency. In addition, the mean ISR is overestimated because the steady-state gain predicted by the 2E model underestimates the true one, *i.e.*, the area under $g^m(t)$ is less than that under $g^t(t)$. Figure 2 (bottom panel) shows the difference between the simulated response to a glucose stimulus of Fig. 1C and the deconvoluted ISR (for clarity we show $\hat{u} - u$ instead of $\hat{u}$ *vs.* u which would have appeared too close in the first minutes). Although the estimation error is significant around the major peak ($0 < t < 20$ min), the 2E model provides a good reconstruction of the second phase ISR ($t > 20$ min) because the low-medium frequency system spectrum is modeled quite well. However, the basal ISR ($t < 0$ min) is overestimated. Accordingly, the 2E model provides a satisfactory reconstruction of ultradian oscillations, except for an overestimation of the mean ISR (not shown).

One Exponential Model. Figure 3 (top-left panel) shows the 1E model fit against the simulated samples. Figure 3 (top-right panel) shows the time course of $g^m(t)$ and $g^t(t)$. The use of the 1E model leads to unsuccessful results in all three ISR problems. In fact, the 1E model provides a bad description of the system spectrum in every range of frequency. In particular, even the low-frequency components of the estimated inputs (mean and slow trends) are affected by gross errors. Figure 3 (middle panel) compares the deconvoluted ultradian oscillations profile with the true one. Note that even the mean ISR is badly estimated. Similar results have been obtained for the reconstruction of rapid pulses (not shown). Fig. 3 (bottom panel)

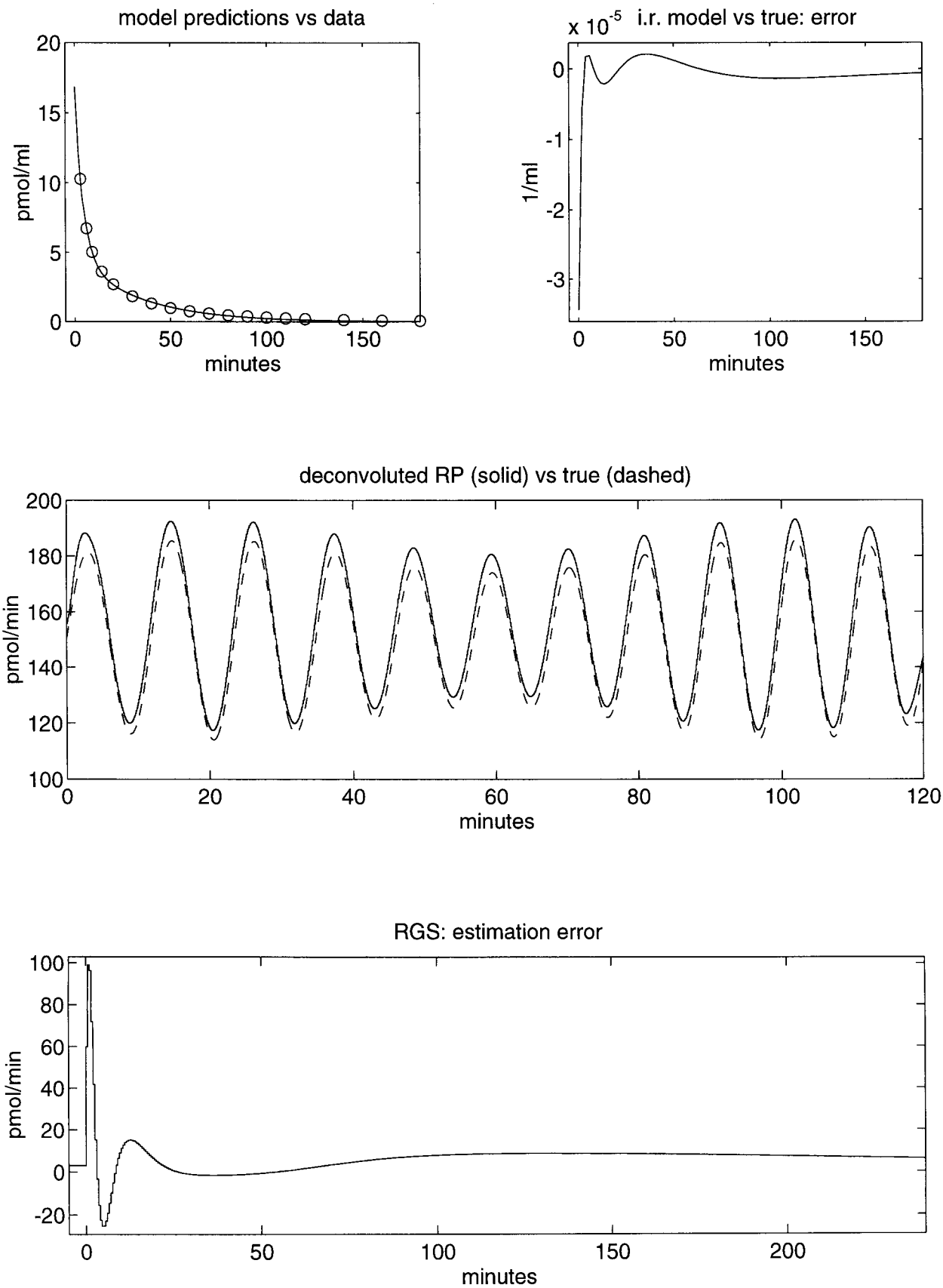

FIGURE 2. Bolus input and 2E model. (top-left) Model predictions (solid line) *versus* data (open bullets). (top-right) Difference between $g^m(t)$ and $g^t(t)$. (middle) Deconvoluted RP (solid line) *versus* true (dotted line). (*bottom*) Difference between the deconvoluted RGS and the true insulin secretion rate (ISR).

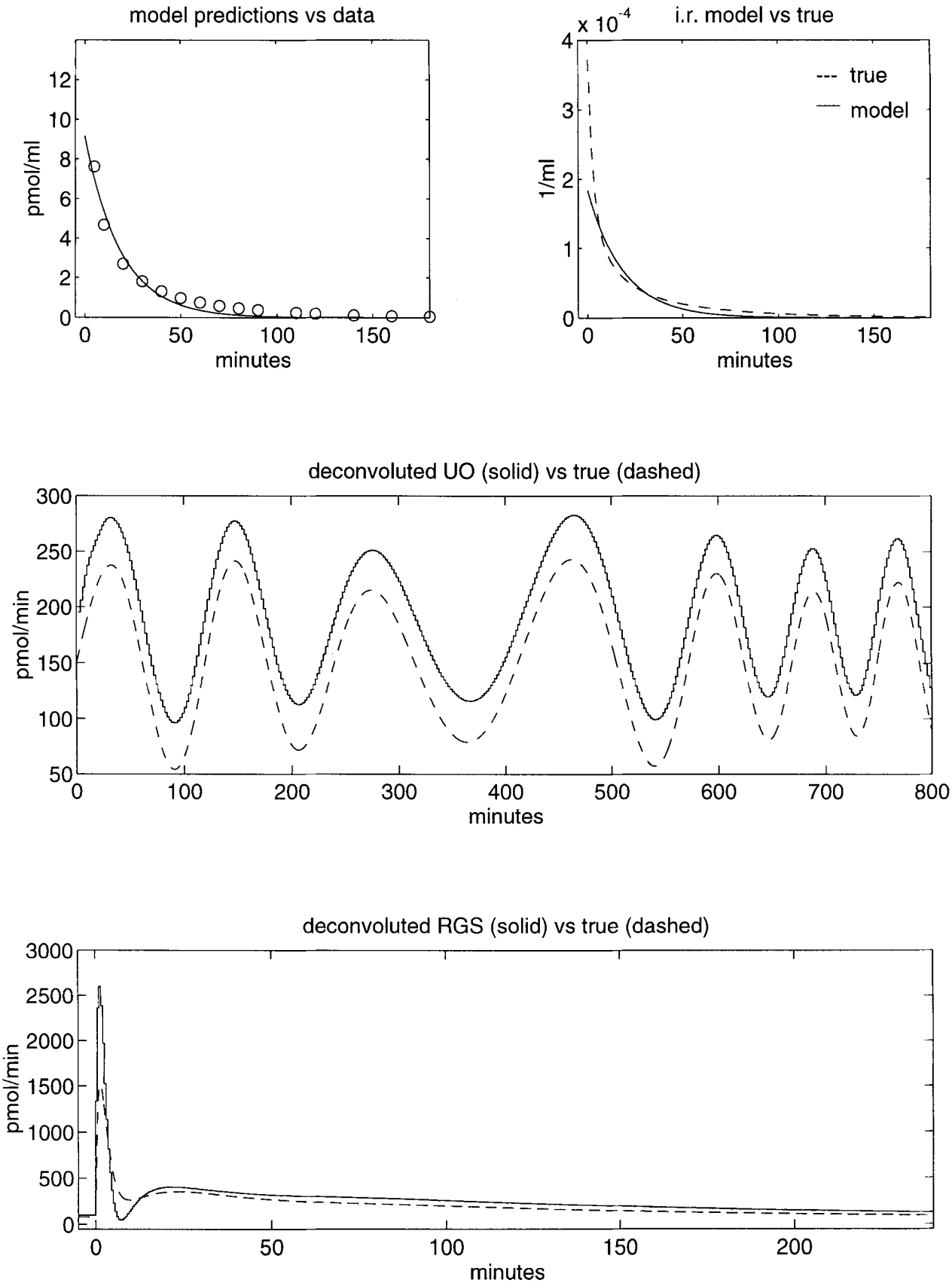

FIGURE 3. Bolus input and 1E model. (top-left) Model predictions *versus* data. (top-right) Time course of $g^m(t)$ (solid line) *versus* (t) (dotted line). (middle) Deconvoluted UO *versus* true (bottom) Deconvoluted RGS *versus* true.

shows the deconvoluted response to a glucose stimulus *versus* the true one. Note how the inaccuracy of the model causes gross errors in the high-frequency components of the deconvoluted input.

Conclusions. The 1E model works badly in every situation. As a matter of fact, the frequency response of the 1E model is far from that of the true system even at low frequency and, in particular, the steady-state gain is grossly wrong. Figure 4 compares the frequency response of the 1E model (dashed line) with that of the true system (continuous line) for $T = 10$ (top panel) and for $T = 2$ (middle panel). On the contrary, the 2E model provides a quite satisfactory description of the system frequency response, at least at low-medium frequency, as displayed by Fig. 4 for $T = 10$ (bottom panel, dashed line); note the closeness for $0.002 < \nu < 0.009\ \text{min}^{-1}$ and the discrepancy for $\nu > 0.01\ \text{min}^{-1}$. However, the 2E model does not predict the correct steady-state gain (see value at $\nu = 0$) and thus wrongly estimates the basal ISR. In summary, the major lesson learned here is that if model identification is based on the response to a bolus (whose spectrum is a constant) it is difficult to track even the low-frequency spectral content of the system with an underparameterized model.

Step Input for Impulse Response Identification

Contrary to the bolus input, whose spectrum is a constant, the major spectral content of a step function is concentrated at low frequencies (9,13). The use of a step as input for impulse response identification should thus allow easier tracking of at least the low-frequency spectral content of the system. An impulse response identification experiment was thus simulated in which the response to a step, *i.e.*, a constant CP infusion, is measured. Then 1E, 2E, and 3E models are fitted against the simulated sampled data. Again, each model has its own sampling schedule Ω_s. In the Appendix, as with the bolus input, we report the rate of infusion, the sampling schedules used for the three models, and the value of the estimated impulse response parameters together with the values of the other system kinetic parameters.

Three Exponential Model. The performance of the 3E model is still excellent in all three ISR problems (results not shown). However, it is worth speculating that, in the presence of noise, it could be difficult to detect accurately the fastest mode of the system from the response to a step.

Two Exponential Model. Figure 5 (top-left panel) shows the 2E model fit against the simulated samples. Note that the steady-state gain predicted by the model is very close to the true one (see Table 1) so that the plateau is well predicted. Figure 5 (top-right panel) reports the difference between the 2E impulse response model $g^m(t)$ and $g^t(t)$. Note that the difference between the first portion of the two curves, say for $t < 3$ min, is even larger than that of the bolus case (Fig. 2, top-right). Figure 5 (middle panel) displays the deconvoluted rapid pulses *versus* the true ones and highlights, again, the deficiency of the 2E model at high frequency. Figure 5 (bottom panel) shows the difference between the true response to a glucose stimulus and the deconvoluted ISR. (Again, for clarity of the picture we show $\hat{u} - u$ instead of $\hat{u}$ *vs.* u.) Note that, although the basal and slow trends of ISR are estimated more accurately than in the bolus case (compare the estimation error for $t < 0$ and for $t > 20$ with that of Fig. 2, bottom panel), the peak after the glucose stimulus is even more overestimated. As expected, the 2E model perfectly reconstructs ultradian oscillations (not shown).

One Exponential Model. Figure 6 (top-left panel) shows the 1E model fit. Figure 6 (top-right panel) compares the 1E impulse response model $g^m(t)$ with $g^t(t)$. Figure 6 (middle panel) shows the deconvoluted ultradian oscillations *versus* the true ones. The performance of the 1E model is now much more satisfactory than in the bolus case. However, the 1E model is grossly deficient at high frequency, and it fails to reconstruct the rapid pulses and the response to a glucose stimulus. Figure 6 (bottom panel) shows the deconvoluted response to a glucose stimulus *versus* the true one; note how the underestimation of the high-frequency system spectral content results in an overestimation of the high-frequency ISR components, also causing negative ISR estimates. Because noise-free data are used in this paper, the reason for the negative estimates is clear. If the data had been noisy, one would have been tempted to formulate a different (and wrong) cause for such negative estimates, *i.e.*, the ill conditioning of the deconvolution problem.

Conclusions. The lesson here is that the use of the step input for impulse response identification provides a model whose low-frequency spectrum is very close to that of the true system, despite the fact that the impulse responses can be very different in the time domain (see Figs. 5 and 6, top-right panels). In particular, the steady-state gain of the models is satisfactorily close to the true one (see Table 1). However, underparameterized models still lack in matching the high-frequency content of the true system spectrum $G^t(e^{j2\pi\nu T})$ (especially for T small). Figure 4 (top panel) compares the

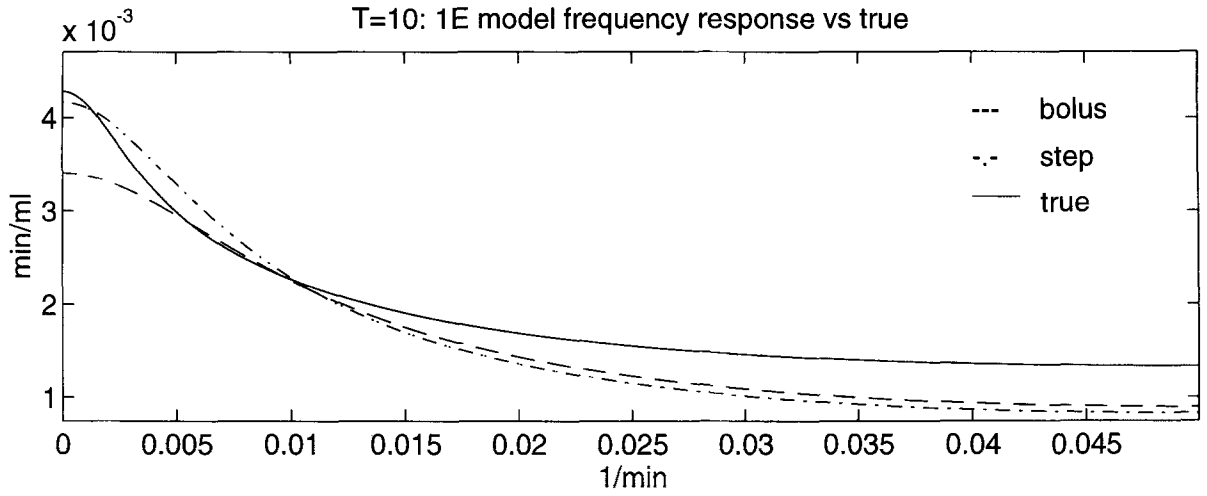

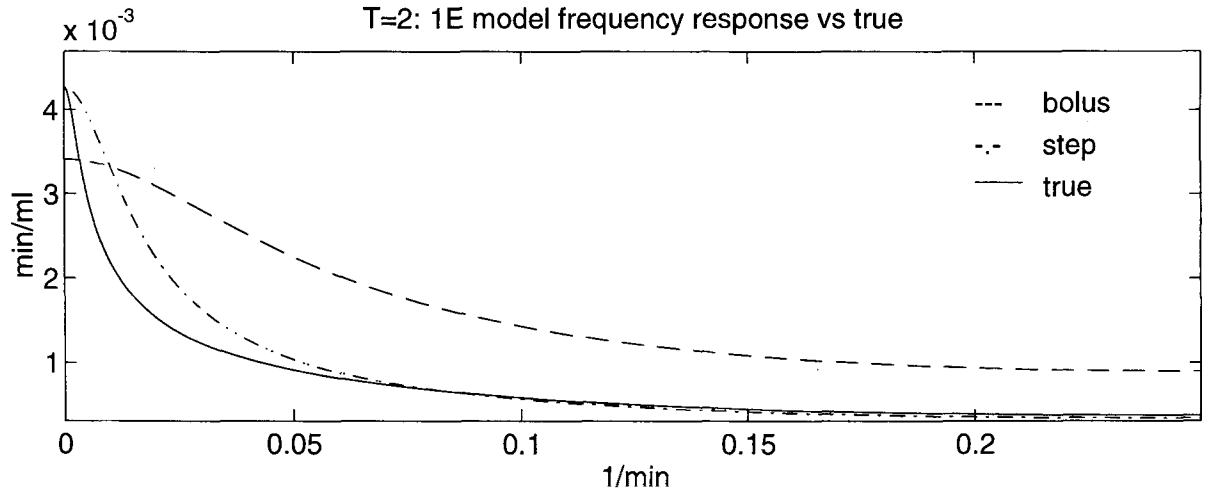

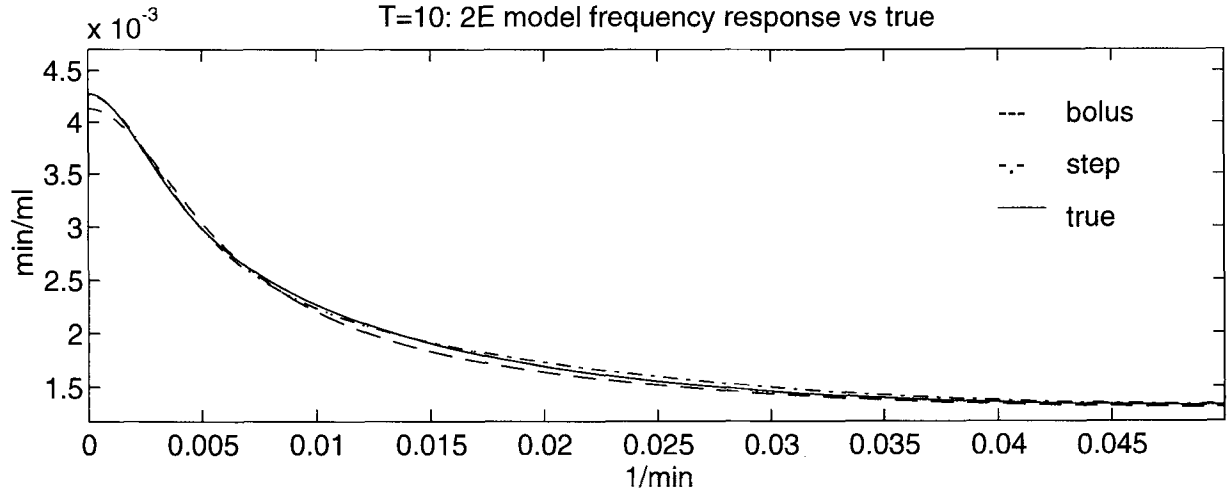

FIGURE 4. Modulus of the frequency response of the discrete-time system (continuous line) *versus* that of models. (top) $T = 10$. 1E model fitted against the bolus (dashed line). 1E model fitted against the step (dashed-dot line). (middle), $T = 2$. 1E model fitted against the bolus (dashed line). 1E model fitted against the square-wave (dashed-dot line). (bottom) $T = 10$. 2E model fitted against the bolus (dashed line). 2E model fitted against the step (dashed-dot line).

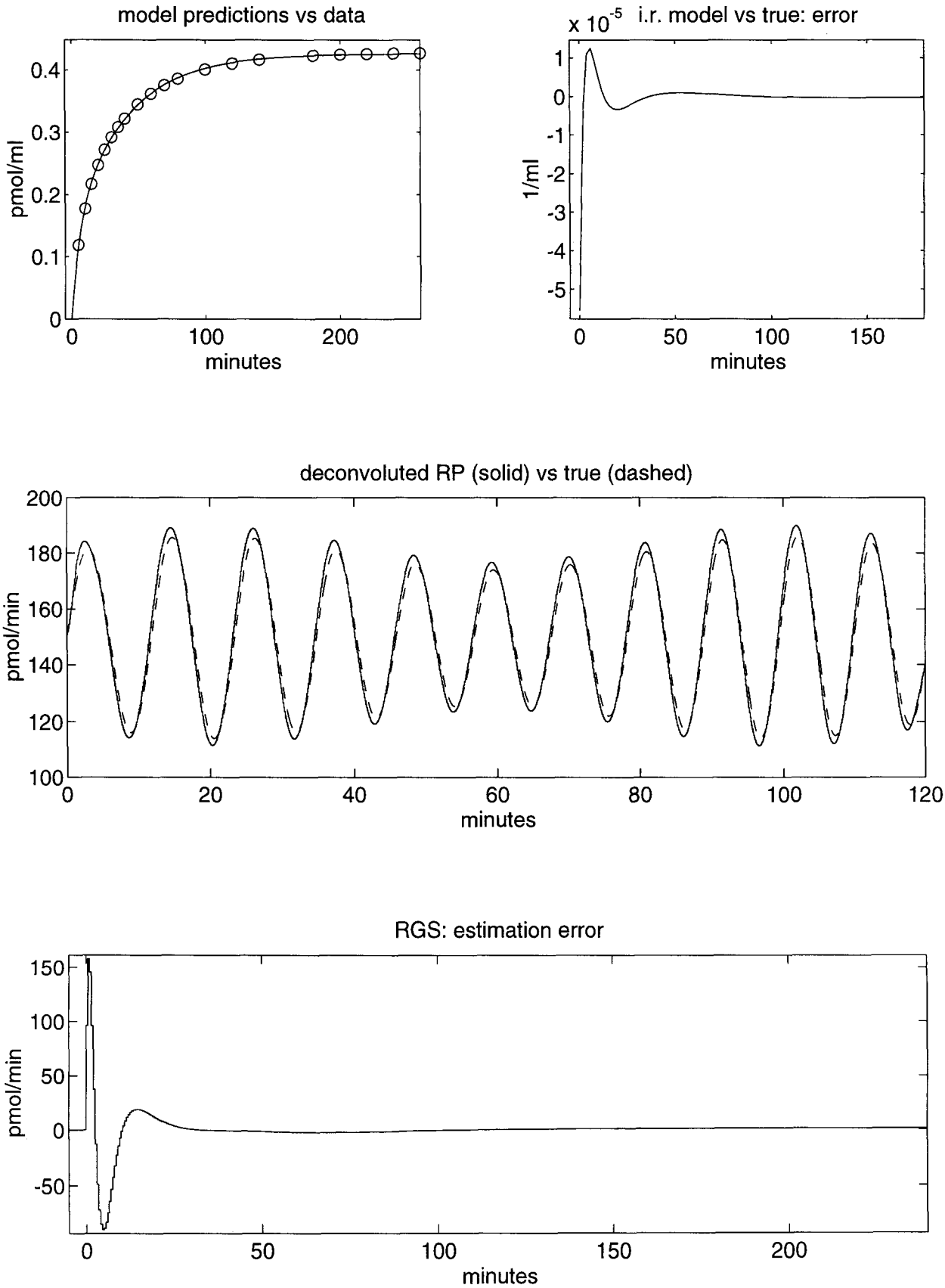

FIGURE 5. Step input and 2E model. (top-left) Model predictions *versus* data. (top-right) Difference between $g^m(t)$ and $g^t(t)$. (middle) Deconvoluted RP *versus* true. (bottom) Difference between the deconvoluted RGS and the true ISR.

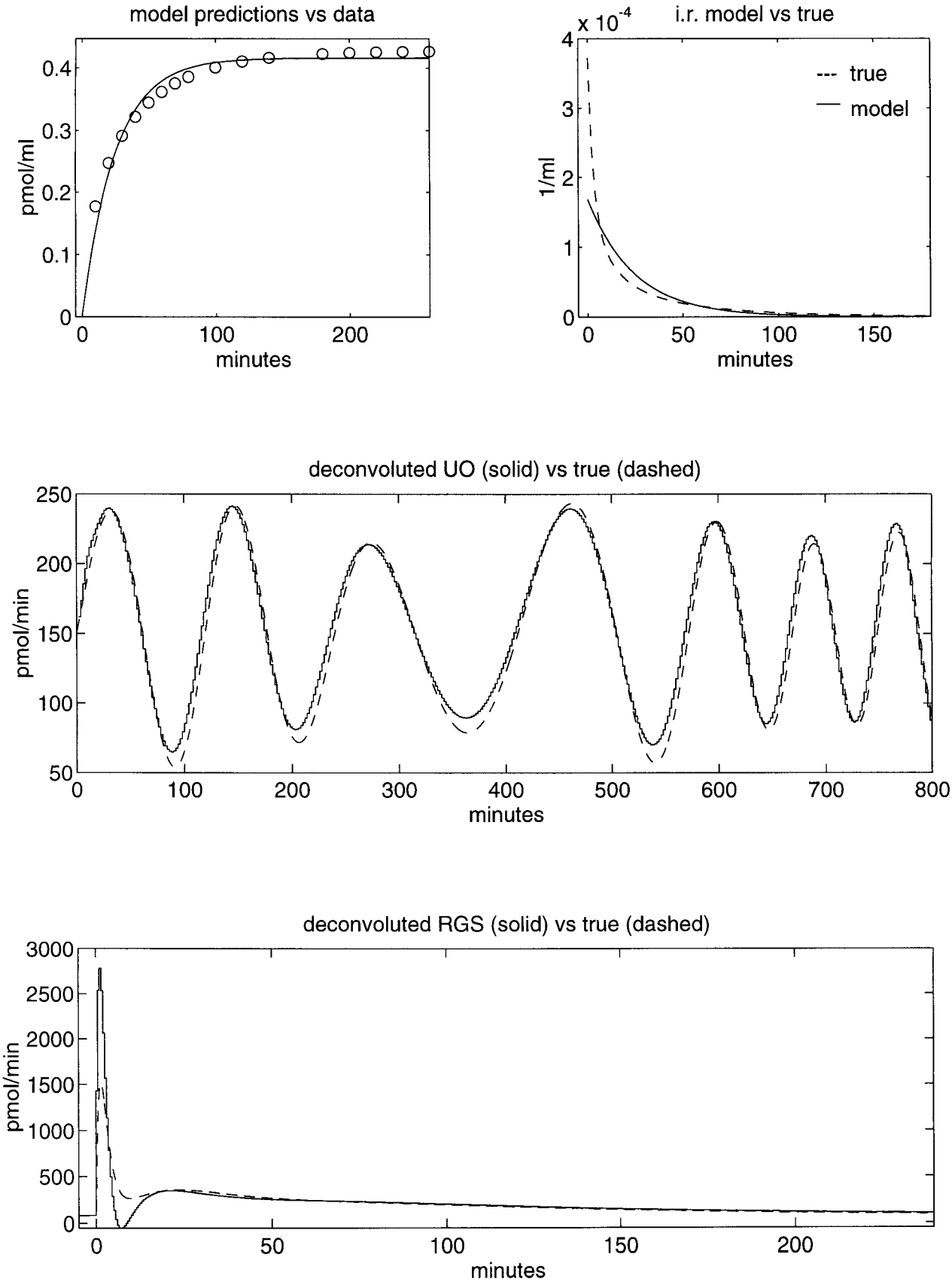

FIGURE 6. Step input and 1E model. (top-left) Model predictions *versus* data. (top-right) Time course of $g^m(t)$ *vs* $g^t(t)$. (middle) Deconvoluted UO *versus* true. (bottom) Deconvoluted RGS *versus* true.

frequency response of the discrete-time 1E model (dashed-dot line) with that of the true system (continuous line) for $T = 10$. Note, especially for $\nu < 0.003$ min^{-1}, the improved description of the system frequency response provided by the 1E model fitted against the step *versus* that fitted against the bolus (dashed line). Figure 5 (bottom panel) compares the frequency response of the 2E model (dashed-dot line) with that of the true system (continuous line) for $T = 10$. Note that the 2E model well describes the system frequency response for $\nu < 0.02$ min^{-1}. Its performance deteriorates at high frequency, *i.e.*, for $\nu > 0.025$ min^{-1}.

Square Wave Input for Impulse Response Identification

In the preceding paragraph we showed that a suitably identified 1E model can work quite well at low frequency and it thus has the chance to provide a reliable reconstruction of ISR slow changes, *e.g.*, ultradian oscillations. However, the 1E model can also provide accurate estimates for rapid pulses. To show this, we forced the system by a constant infusion followed by four square waves with a 12 min period. We then fitted 1E, 2E, and 3E models against output samples collected every 2 min by nonlinear least squares. In the Appendix, we report the rate of infusion, the sampling schedules, and the value of the estimated impulse response parameters together with the values of the other system kinetic parameters.

Three Exponential Model. The 3E model was not resolvable. The spectrum of the square wave is a sequence of lines located at the multiples of the fundamental frequency 1/12. Thus, the input does not excite the system at frequencies less than 1/12, and the slowest mode of the 3E model cannot be fitted.

Two Exponential Model. The 2E model performance is excellent for rapid pulses, but it is not satisfactory for ultradian oscillations and for the second phase response to a glucose stimulus (results not shown).

One Exponential Model. Figure 7 (top-left panel) shows the 1E model fit. Figure 7 (top-right panel) shows the time course of the 1E model impulse response $g^m(t)$ *versus* that of $g^t(t)$. Figure 7 (middle panel) displays the deconvoluted rapid pulses when this 1E model is used *versus* the true input. Apart from the small phase lag, this 1E model is suitable to reconstruct rapid pulses. In addition, the mean ISR is correct. In contrast, the model fails in reconstructing slow trends, *e.g.*, ultradian oscillations and very fast transients. Figure 7 (bottom panel) displays the deconvoluted response to a glucose stimulus *versus* the true one. Note that, although the peak estimation is reasonable, there are gross errors in the second phase reconstruction.

Conclusions. The square wave input above leads the frequency response of the models $G^m(e^{j2\pi\nu T})$ to have the correct steady-state gain (see Table 1) and to be similar to the true system spectrum $G^t(e^{j2\pi\nu T})$ in the frequency range in which the rapid pulses spectrum lies. On the contrary, the models are not able to match the system spectrum at low frequency. Figure 4 (middle panel) displays, for $T = 2$, the frequency response of the true system (continuous line) *versus* that of the 1E model fitted against the square-wave (dashed-dot line) and that of the 1E model fitted against the bolus (dashed line). Note that the 1E model fitted against the square-wave describes very well the system frequency response for $0.07 < \nu < 0.12$ min^{-1}. Its performance is rough at low frequency, *i.e.*, for $\nu < 0.06$ min^{-1}, but it predicts the system steady-state gain correctly.

Better Inputs for Impulse Response Identification

So far, we have considered standard inputs for impulse response identification and have seen that the use of the step and the square wave input allowed the model to match the frequency response of the system in certain frequency bands. However, from a theoretical point of view, these inputs are not the best to calibrate, in a given frequency band, the frequency response of a model against that of the system. Ideally, one could resort to a technique in which the input for impulse response identification is obtained by bandpass filtering a Dirac pulse. This input excites the system in a well-defined frequency band only so that, in the parameter estimation procedure, the model will not have to track data outside the selected frequency band.

In practice, it is obviously unfeasible to implement the above-mentioned theoretical identification strategy. However, some simple, even nonstandard inputs can be designed and used to improve the description of the system frequency response in a certain band. For instance, the low-frequency spectrum of the system can be better evidenced by using a ramp infusion followed by a constant. The smaller the slope of the ramp, the easier it is to observe the low-frequency content of the system spectrum. We applied this input to the system described by $g^t(t)$ and identified a 1E model from the samples of the simulated system response. The sampling schedule is reported in the Appendix together with the values of the system parameters. Figure 8 (top-left panel) shows the 1E model fit. This fit is better than that of the step input (Fig. 6, top-left).

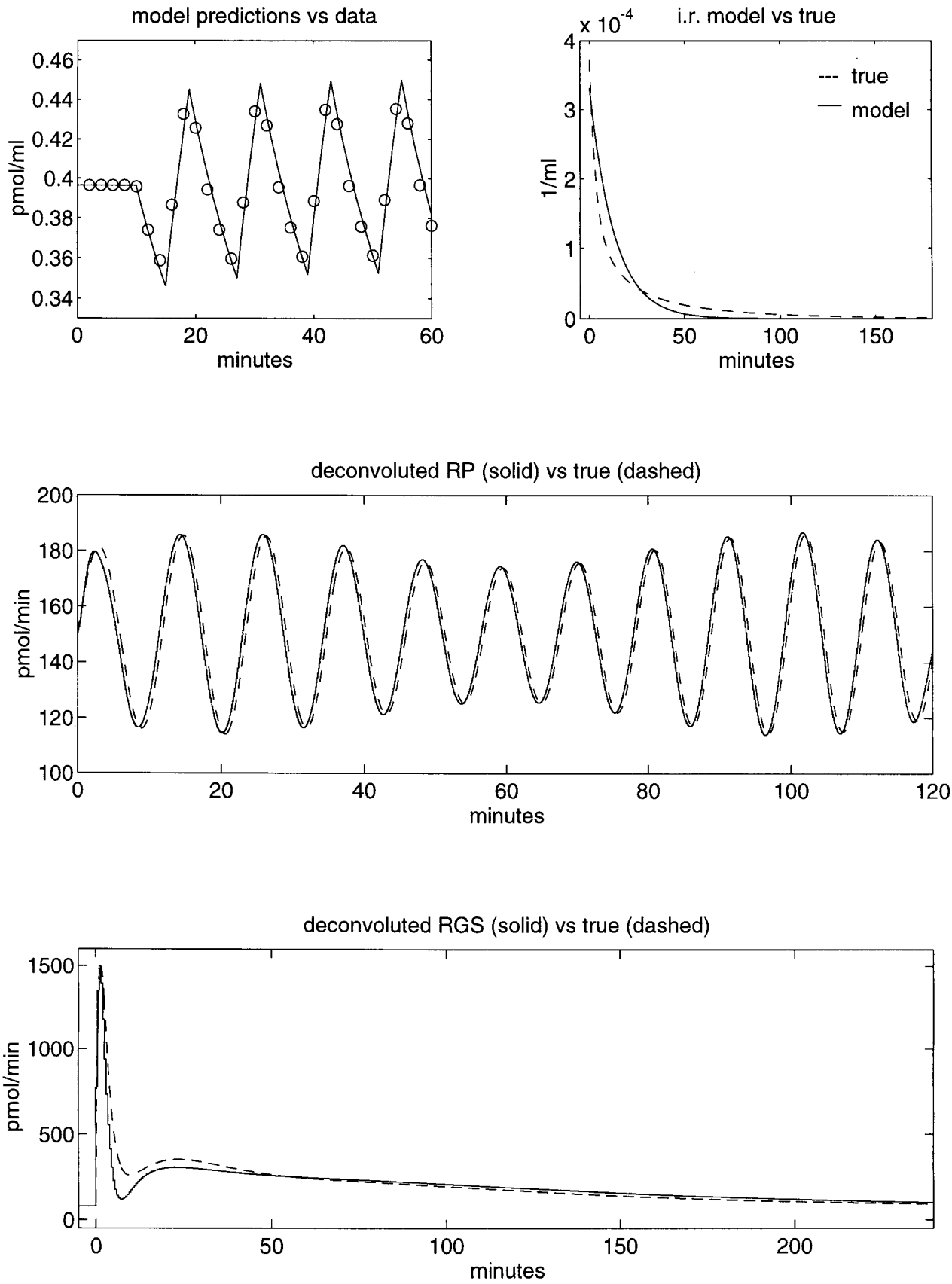

FIGURE 7. Square-wave input and 1E model. (top-left) Model predictions *versus* data. (top-right) Time course of $g^m(t)$ *versus* $g^t(t)$. (middle) Deconvoluted RP profile *versus* true. (bottom) Deconvoluted RGS *versus* true.

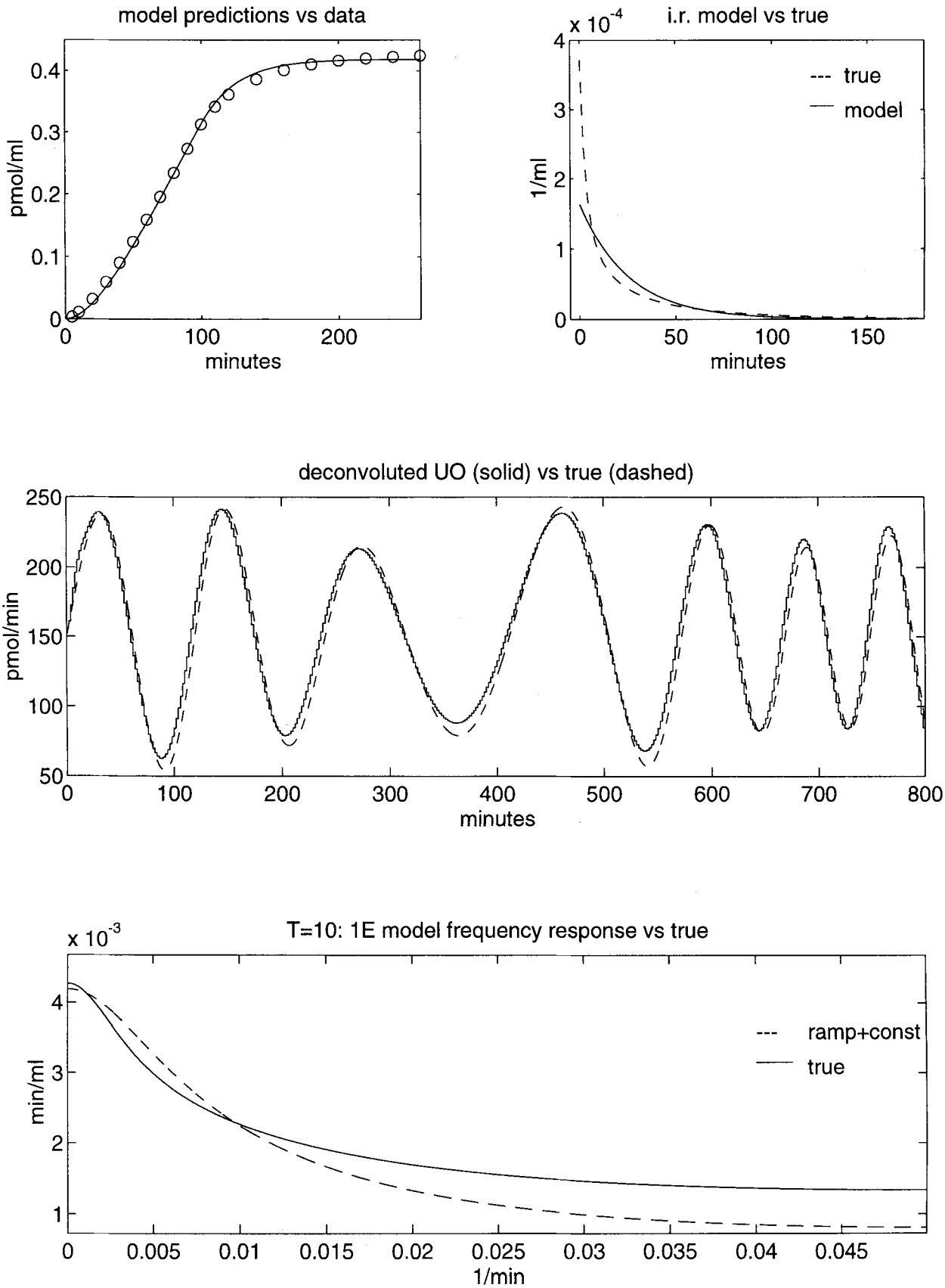

FIGURE 8. "Ramp + constant" input and 1E model. (top-left) Model predictions *versus* data. (top-right) Time course of $g^m(t)$ *versus* $g^t(t)$. (middle) Deconvoluted UO *versus* true. (bottom) Modulus of the frequency response of the 1E model (dashed line) *versus* system (continuous line) for $T = 10$.

Figure 8 (top-right panel) highlights the differences between $g^m(t)$ and $g^t(t)$. Figure 8 (middle panel) shows the performance of the 1E model in reconstructing ultradian oscillations. It is only slightly better than that of the 1E model identified from the step input (Fig. 6, bottom panel). In fact, the frequency response of the two models is similar; Figure 8 (bottom panel) displays this 1E model frequency response *versus* that of the true system for $T = 10$ (compare with Fig. 4, top panel). However, an advantage of the "ramp + constant" input is that, with real noisy data, the estimation of model parameters would be more robust than that with the step input.

REAL DATA SUPPORT SIMULATION RESULTS

In this paper we use real data to suppor the predictions obtained by simulation. A full test of the various combinations is not possible because only one input, usually the standard CP bolus, has been used for impulse response identification in the literature. Thus we do not have square wave and step data to compare with the bolus data in the same subject. However, we have developed a reasonable strategy which makes full use of available data and allows us to assess with confidence the simulation predictions. Because real data are used to perform deconvolution, which is now sensitive to ill conditioning because of the measurement error, we switched to the regularization algorithm presented in (22), which can also be viewed as the adaptation of the algorithm presented in (5) to ill-conditioned problems.

Response to a Glucose Stimulus

We consider the data of Subject 3 in (22), a normal human being, originating from the two-stage experiment (20). An intravenous bolus of CP was injected to determine the impulse response which was best described by a 3E model (22), which will be denoted by $g^t(t)$. The same person was then observed after a glucose stimulus, *i.e.*, 0.5 g/kg of body weight of glucose are injected into the plasma and CP concentrations are measured for 4 hr on a nonuniform grid. Measurement error of CP data is uncorrelated, normal, with zero mean and a constant but unknown coefficient of variation (CV). In Figure 9 (top-left) we show the deconvoluted ISR obtained with the 3E model. The deconvolution algorithm used here is the same as in (22). Figure 9 (bottom-left) shows the reconvolution profile against the CP data. From $g^t(t)$ we have then simulated a step response from which, as under "Step Input for Impulse Response Identification", we have obtained a 1E model g^m(t) (not shown). Figure 9 (top-right) shows the deconvoluted profile obtained with this 1E model. Figure 9 (bottom-right) shows the reconvolution profile against the CP data. These results (and those obtained by using the 1E and 2E models identified from the other inputs and not shown in the paper) fully support the simulation predictions.

Ultradian Oscillations

We consider the data of Subject 1, a normal man, originating from the two-stage experiment (23). An intravenous bolus of CP was injected in the plasma to determine the impulse response. In our hands, data are again best modeled by a 3E model denoted by $g^t(t)$. In the same person, a CP plasma concentrations time series was obtained by collecting samples every 10 min for 20 hr in the presence of a constant glucose infusion. Measurement error of CP data is uncorrelated, normal with zero mean, and a constant CV of 5%. Figure 10 (top-left) shows the ultradian oscillations profile obtained by deconvolving the CP data with the 3E impulse response model $g^t(t)$. Figure 10 (top-right) shows the reconvolution profile against the CP data. From $g^t(t)$ we have then simulated the response to the "ramp + constant" input of "Better Inputs for Impulse Response Identification" and fitted a 1E impulse response model, $g^m(t)$ (not shown). Figure 10 (bottom-left) shows the deconvoluted profile obtained with this 1E model. Figure 10 (bottom-right) shows the reconvolution profile against the CP data. These results (and those obtained by using the 1E and 2E models identified from the other inputs and not shown in the paper) are again in line with the simulation predictions.

CONCLUSIONS

The CP concentration measured in plasma allows the reconstruction of insulin secretion rate by deconvolution. Deconvolution requires knowledge of the CP impulse response. A two exponential model is usually chosen to describe the CP impulse response but three exponential and one exponential models have also been used. The purpose of this work was to investigate the role of the CP impulse response model order in reconstructing ISR by deconvolution in three classical physiological situations. The simulations showed that, in deconvolution, the difference between the frequency response of the model and that of the system is of crucial importance, not the difference between the time courses of their impulse responses. In fact, we have shown that, although the time course of the impulse response of the model can be very different from that of the system, their frequency responses can

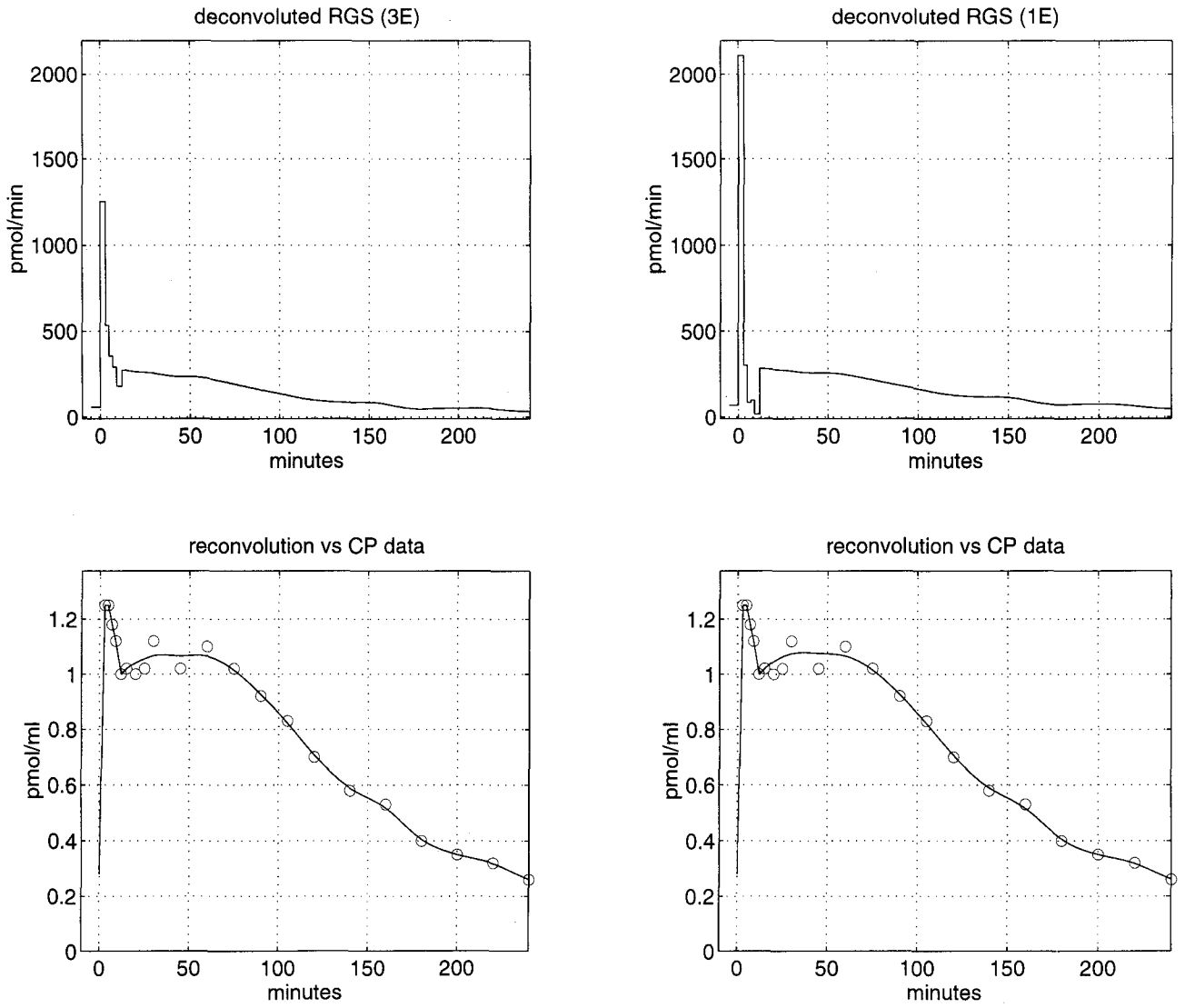

FIGURE 9. Real RGS data. (top-left) Deconvoluted RGS (3E model fitted against the bolus). (bottom-left) Reconvolution *versus* CP data. (top-right) Deconvoluted RGS (1E model fitted against the step). (Bottom-right) Reconvolution *versus* CP data.

be much more similar, at least in a limited frequency band. However, it is clear that the simpler the impulse response model, the less complex the frequency response of the system is which can be described correctly. Although the spectrum of the discretized system depends on the sampling rate, the model frequency response heavily depends on the form of the input chosen in the identification experiment.

In this work, a 1E impulse response model has been shown to have the chance to perform satisfactorily if the spectrum of the ISR is concentrated in a narrow band, as it happens for ultradian oscillations and rapid pulses. However, to work well, its parameters must derive from a suitably designed input-output experiment, *e.g.*, using a square wave input. On the other hand, at least a 2E model is needed to satisfactorily (possibly very well) reconstruct a complex ISR pattern like the response to a glucose stimulus. Tests with real data have been confirmatory. Therefore, from this work it follows that input estimation techniques using a 1E model (26–28) are likely to provide questionable results, especially for the reconstruction of ISR after a glucose stimulus. This agrees with the conclusions drawn in (24,25) which were mostly developed on an empirical basis.

From this study it may seem that a 3E model should be preferred, especially for reconstructing the response to a glucose stimulus. However, we recommend its use only when the 3E model is definitely superior to the 2E model in model fitting. Otherwise, because overparameterization makes models overly sensitive to noise in the data, the high-frequency spectral content

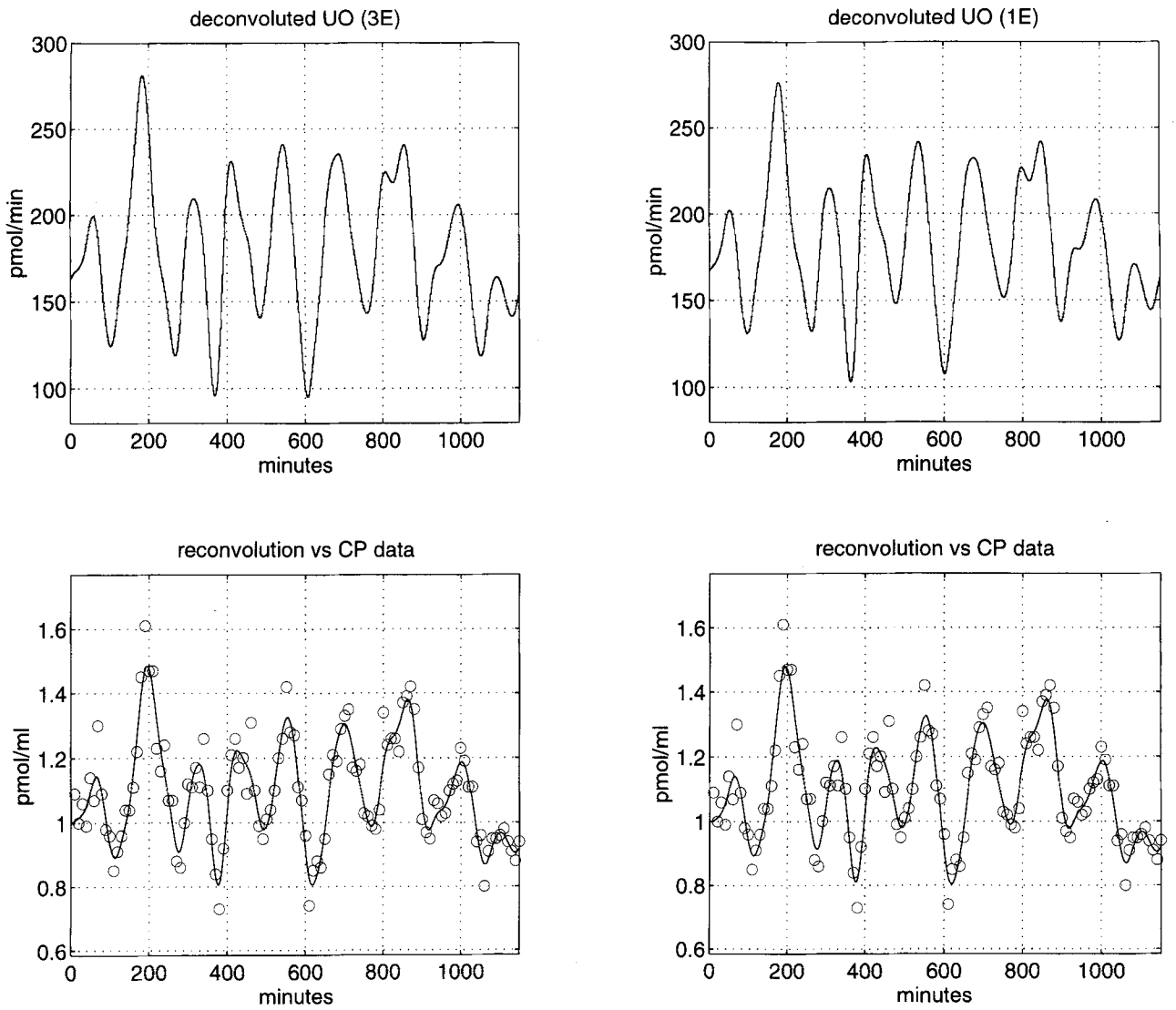

FIGURE 10. Real UO data. (top-left) Deconvoluted UO (3E model fitted against the bolus). (bottom-left) Reconvolution *versus* CP data. (top-right) Deconvoluted UO (1E model fitted against the ramp + constant). (bottom-right) Reconvolution *versus* CP data.

of $g^m(t)$ may overestimate that of the true $g^t(t)$. All our simulations have been based on real subject three exponential impulse response models which were judged superior by classical model order selection criteria (11).

The use of noise-free data has allowed us to make an analysis not confounded by the ill conditioning of the deconvolution problem. When data are noisy, regularization techniques are needed to filter noise from the true signal. Because regularization techniques intrinsically attenuate ISR high frequencies, the theoretical advantages of the 3E model become less and less as more regularization is needed.

The simulated deconvolution problems have been studied intentionally in the absence of noise to specifically address the issue of *accuracy* of the input estimate *versus* impulse response model error. In practice, an additional issue arises, that is the *precision* of the input estimate. In a real deconvolution problem there are two sources of error: measurement error in the deconvolution data and impulse response parameters uncertainty (arising from the fact that identification data are noisy). To simultaneously take into account the influence of both factors in the assessment of the confidence intervals of the input estimate, one must resort to a Monte Carlo simulation, see (22) for example, in which ISR after a glucose stimulus was reconstructed. In general, the role of impulse response parameters uncertainty depends on the particular system studied and obviously increases as measurement error in the identification data gets larger and larger. The lower the model order is, the less uncertain the impulse response

parameters become and thus the less influence this uncertainty has in determining the deconvolution confidence bands. However, the lower the model order is, the higher the risk of loosing accuracy becomes, because of the greater possibility that bias errors caused by impulse response undermodeling arise.

To conclude, even when underparameterized models work well, *e.g.*, the 1E model identified from the square wave input for reconstructing rapid pulses, they can predict system parameter values that are either untrue or unphysiological, *e.g.*, in Table 1, compare the model-predicted values of steady-state gain, plasma volume, and mean residence time with the true ones. In fact, the system parameters are influenced by the entire time course of the system impulse response or, in other words, by the entire system frequency response, whereas the (possibly good) performance of an underparameterized model is linked to its (possibly good) frequency behavior in a somewhat limited band. Hence, even when they work, underparameterized models should be simply interpreted as (black-box) models of the input-output behavior of the system against a certain kind of discrete-time signals rather than models (with physiological meaning of the parameters) of the continuous-time system impulse response.

REFERENCES

1. Carson, E., C. Cobelli, and L. Finkelstein. *The Mathematical Modeling of Metabolic and Endocrine Systems.* New York: John Wiley and Sons, 1983.
2. Cobelli, C., A. Ruggeri, J. J. Di Stefano II, and E. M. Landaw. Optimal design of multioutput sampling schedules. Software and applications to endocrine-metabolic and pharmacokinetic models. *IEEE Trans. Biomed. Eng.* 32:249–256, 1985.
3. D'Argenio, D. Z. Optimal sampling times for pharmacokinetic experiments. *J. Pharmacokinet. Biopharm.* 9:739–756, 1981.
4. De Nicolao, G., and D. Liberati. Linear and nonlinear techniques for the deconvolution of hormone time-series. *IEEE Trans. Biomed. Eng.* 40:440–455, 1993.
5. De Nicolao, G., D. Liberati, and A. Sartorio. Deconvolution of infrequently sampled data for the estimation of growth hormone secretion. *IEEE Trans. Biomed. Eng.* 42:678–697, 1995.
6. Eaton, R. P., R. C. Allen, D. S. Schade, K. M. Erickson, and J. Standefer. Prehapatic insulin production in man: Kinetic analysis using peripheral connecting peptide behaviour. *J. Clin. Endocrinol. Metab.* 51:520–528, 1980.
7. Faber, O. K., C. Hagen, C. Binder, J. Markussen, V. K. Nahitani, P. M. Blix, H. Kuzuya, D. L. Horwitz, A. H. Rubenstein, and N. Rossing. Kinetics of human connecting peptide in normal and diabetic subjects. *J. Clin. Invest.* 62:197–202, 1979.
8. Hansen, B. C., K. L. Jen, S. B. Pek, and R. A. Wolfe. Rapid oscillations in plasma insulin, glucagon, and glucose in obese and normal weight humans. *J. Clin. Endocrinol. Metab.* 54:785–792, 1982.
9. Hsu, H. P. *Outline of Fourier Analysis.* New York: Unitech Division, 1967.
10. Lang, D. A., D. R. Matthews, D. Phil, J. Peto, and R. C. Turner. Cyclic oscillations of basal plasma glucose and insulin concentrations in human beings. *N. Engl. J. Med.* 301:1023–1027, 1979.
11. Landaw, E. M., and J. J. DiStefano III. Multiexponential, multicompartmental, and noncompartmental modeling. II. Data analysis and statistical considerations. *Am. J. Physiol.* 246:R665–R677, 1984.
12. Oppenheim, A. V., and R. W. Schafer. *Digital Signal Processing.* Englewood Cliffs, NJ: Prentice and Hall, 1975.
13. Papoulis, A. *The Fourier Integral and Its Applications.* New York, NY: McGraw-Hill, 1962.
14. Pilo, A., E. Ferrannini, and R. Navalesi. Measurement of glucose-induced delivery rate in man by deconvolution analysis. *Am. J. Physiol.* 233:E500–E508, 1977.
15. Polonsky, K. S., and A. H. Rubenstein. C-peptide as a measure of the secretion and hepatic extraction of insulin: Pitfalls and limitations. *Diabetes* 33:486–494, 1984.
16. Polonsky, K. S., J. Licinio-Paixao, B. D. Given, W. Pugh, P. Rue, J. Galloway, T. Karrison, and B. Frank. Use of biosynthetic human C-peptide in the measurement of insulin secretion rates in normal volunteers and type I diabetic patients. *J. Clin. Invest.* 77:98–105, 1986.
17. Polonsky, K. S., B. D. Given, and E. Van Cauter. Twenty-four-hour profiles and pulsatile patterns of insulin secretion in normal and obese subjects. *J. Clin. Invest.* 81:442–448, 1988.
18. Rubenstein, A. H., L. A. Pottenger, M. Mako, G. S. Getz, and D. F. Steiner. The metabolism of insulin and proinsulin by the liver. *J. Clin. Invest.* 51:912–920, 1972.
19. Shapiro, E. T., H. Tillil, K. S. Polonsky, V. S. Fang, A. H. Rubenstin, and E. Van Cauter. Oscillations in insulin secretion during costant glucose infusion in normal man: Relationship to change in plasma glucose. *J. Clin. Endocrinol. Metab.* 67:307–314, 1988.
20. Shapiro, E. T., H. Tillil, A. H. Rubenstein, and K. S. Polonsky. Peripheral insulin parallels changes in insulin secretion more closely than C-peptide after bolus intravenous glucose administration. *J. Clin. Endocrinol. Metab.* 67:1094–1099, 1988.
21. Sparacino, G., J. Sturis, N. O. Meara, M. Byrne, G. De Nicolao, K. Polonsky, and C. Cobelli. A deconvolution method to quantify rapid pulses in insulin secretion. In: *Proceedings of Annual International Conference of the IEEE Engineering in Medicince and Biology Society,* vol. 15, edited by A. Szeto and R. Rangayyan. San Diego, CA: 1993, pp. 536–537.
22. Sparacino, G., and C. Cobelli. A stochastic deconvolution method to reconstruct insulin secretion rate after a glucose stimulus. *IEEE Trans. Biomed. Eng.* 43:512–529, 1996.
23. Sturis, J., E. Van Cauter, J. D. Blackman, and K. S. Polonsky. Entrainment of pulsatile insulin secretion by oscillatory glucose infusion. *J. Clin. Invest.* 87:439–445, 1991.
24. Toffolo, G., F. De Grandi, and C. Cobelli. Estimation of beta cell sensitivity from IVGTT C-peptide data. Knowledge of the kinetics avoids errors in modeling the secretion. *Diabetes* 44:845–854, 1995.
25. Van Cauter, E., F. Mestrez, J. Sturis, and K. S. Polonsky. Estimation of insulin secretion rates from C-peptide lev-

els: comparison of individual and standard parameters for C-peptide clearance. *Diabetes* 41:368–377, 1992.
26. Volund, A., K. S. Polonsky, and R. N. Bergman. Calculated pattern of intraportal insulin appearance without independent assessment of C-peptide kinetics. *Diabetes* 36:1195–1202, 1987.
27. Volund, A. Application of stochastic simulations to assess precision and robustness of kinetic models for estimation of insulin secretion. In: *Proceedings of the 2nd IFAC Symposium on Modeling and Control in Biomedical Systems, Galveston, Texas, March 1994,* edited by B. W. Patterson. Madison, WI: Omnipress, 1994, pp. 293–294.
28. Watanabe, R. M., A. Volund, R. Subir, and R. N. Bergman. Prehepatic beta cell secretion during the intravenous glucose tolerance test in humans: Applications of a combined model of insulin and C-peptide kinetics. *J. Clin. Endocinrol. Metab.* 69:790–797, 1989.

APPENDIX

The bolus input used for the simulated identification experiments under "Bolus Input for Impulse Response Identification" was $u(t) = D\delta(t)$, where $D = 50{,}000$ pmol. The sampling schedule was $\Omega_s = \{1, 2, 3, 4, 5, 6, 7, 8, 9, 10, 11, 14, 17, 20, 25, 30, 35, 40, 50, 60, 70, 80, 90, 100, 110, 120, 140, 160, 180\}$ for the 3E model, $\Omega_s = \{3, 6, 9, 14, 20, 30, 40, 50, 60, 70, 80, 90, 100, 110, 120, 140, 160, 180\}$ for the 2E model, and $\Omega_s = \{5, 10, 20, 30, 40, 50, 60, 70, 80, 90, 100, 110, 120, 140, 160, 180\}$ for the 1E model.

The step input used for the simulated identification experiments under "Step Input for Impulse Response Identification" was $u(t) = U\delta_{-1}(t)$, where $U = 100$ pmol/min. The sampling schedule was $\Omega_s = \{1, 2, 3, 4, 5, 6, 7, 8, 9, 10, 11, 14, 17, 20, 25, 30, 35, 40, 50, 60, 70, 80, 90, 100, 110, 120, 140, 160, 180\}$ for the 3E model, $\Omega_s = \{5, 10, 15, 20, 25, 30, 35, 40, 50, 60, 70, 80, 100, 120, 140, 180, 200, 220, 240, 260\}$ for the 2E model, and $\Omega_s = \{10, 20, 30, 40, 50, 60, 70, 80, 100, 120, 140, 180, 200, 220, 240, 260\}$ for the 1E model.

The simulated square wave input $u(t)$ under "Square Wave Input for Impulse Response Identification" consisted of 8 min low (56 pmol/min) and 4 min high (168 pmol/min) sequential infusion rates [see (21), subject 1]. The sampling schedule was $\Omega_s = \{kT\}$, where $T = 2$ for both the 1E and 2E models.

The simulated "ramp + constant" input $u(t)$ of under "Better Inputs for Impulse Response Identification" was equal to kt ($k = 1$ pmol/min^2) for $t \leq 100$ min and to 100 pmol/min for $t > 100$ min. The sampling schedule used for the 1E model identification is $\Omega_s = \{5, 10, 20, 30, 40, 50, 60, 70, 80, 90, 100, 110, 120, 140, 160, 180, 200, 220, 240, 260\}$.

Table 1 reports the parameters of the true system together with the values of the parameters of all the impulse response models.

TABLE 1. Values of the impulse response and system kinetic parameters

	A_1 (ml^{-1})	a_1 (min^{-1})	A_2 (ml^{-1})	a_2 (min^{-1})	A_3 (ml^{-1})	a_3 (min^{-1})	K (10^{-3} min/ml)	V (ml)	MRT (min)
True system									
3E	2.23×10^{-4}	0.339	9.46×10^{-5}	0.0790	5.31×10^{-5}	0.0220	4.275	2691	29.68
Model: bolus input									
1E	1.83×10^{-4}	0.0538	–	–	–	–	3.408	5446	18.54
2E	2.43×10^{-4}	0.237	9.38×10^{-5}	0.0302	–	–	4.129	2966	25.91
3E	2.15×10^{-4}	0.352	9.96×10^{-5}	0.0880	5.76×10^{-5}	0.0227	4.273	2682	29.39
Model: Step input									
1E	1.67×10^{-4}	0.0403	–	–	–	–	4.158	5955	24.53
2E	2.45×10^{-4}	0.174	7.11×10^{-5}	0.0249	–	–	4.260	3163	28.63
3E	2.04×10^{-4}	0.387	1.13×10^{-4}	0.0967	5.89×10^{-5}	0.0229	4.270	2653	29.43
Model: square wave input									
1E	3.31×10^{-4}	0.0774	–	–	–	–	4.272	3021	12.89
2E	3.05×10^{-4}	0.239	5.20×10^{-5}	0.017	–	–	4.339	2799	42.75
Model: "ramp + constant" input									
1E	1.63×10^{-4}	0.0390	–	–	–	–	4.189	6111	25.60